Identification and Characterization of Reclaimed and Unreclaimed Mine Features Using Lidar and Temporal Remote Sensing Methods within the Coastal Plain Uranium Mining Region of Texas

Victoria Grace Stengel * , Tanya J. Gallegos , Bernard E. Hubbard , Steven M Cahan , David S Wallace

Posted Date: 30 July 2024

doi: 10.20944/preprints202407.2426.v1

Keywords: Uranium; abandoned mines; reclaimed mines,; Landsat; lidar; Time series; Google Earth Engine

Article

Identification and Characterization of Reclaimed and Underclaimed Mine Features Using Lidar And Temporal Remote Sensing Methods Within the Coastal Plain Uranium Mining Region of Texas

Victoria G. Stengel [1]*, Tanya J. Gallegos [2], Bernard E. Hubbard [1], Steven M. Cahan [1] and D. Sam Wallace [3]

[1] U. S. Geological Survey, Geology, Energy & Minerals Science Center, Reston, VA
[2] U. S. Geological Survey, Mineral Resources Program, Albuquerque, NM
[3] U. S. Geological Survey, Oklahoma-Texas Water Science Center, Fort Worth, TX
* Correspondence: vstengel@usgs.gov

Abstract: Open-pit uranium mining in the south Texas Gulf Coast region was active during the second half of the 20th century. Although some mines have extensive records documenting the locations and extents with descriptions of reclamation procedures and timelines, abandoned and reclaimed mines with minimal documentation concurrently exist where little is known about locations, mine waste volumes, and reclamation status. Advanced mapping of these mining operations is helpful for producing basic mine land inventories and assessments of mine waste; identifying potential undeveloped resources and environmental health issues; and for developing proper management, restoration, and reclamation strategies. We studied known reclaimed and unreclaimed mine sites to develop a spatiotemporal mapping approach utilizing multiple techniques in remote sensing as a proof of concept. A mapping classification system was developed to identify uranium mine waste-rock piles, mine pits (with and without waste water), the total area of land disturbance due to mining, and to differentiate abandoned and reclaimed mine features using lidar (Light Detection and Ranging) analysis and multispectral temporal analysis. Visual interpretation of Landsat imagery and time-series analysis revealed the temporal life-cycle of mining, historical areas of disturbance, and reclamation; however, mine features below vegetation canopies are not always visible in satellite imagery. Lidar laser scanning penetrates the vegetation canopy to measure the topographic elevation and exposes anthropogenic modifications to the landscape. Lidar analysis (bare earth elevation surface, slope, topographic contours, topographic textures, and overland-flow hydrography) revealed mine features, and expansive areas of mining disturbance. The spatiotemporal mapping approach proved to be useful for identifying and characterizing known mine features, areas of disturbance, and reclamation status. Historical pre-mining topographic data were available at only 4 of the mines for comparison where the cut-and-fill tool estimated 21% less waste-rock volume, indicating that information about pre-mining terrain topography and/or subsurface mine waste geometry is needed to improve accuracies for quantifying buried mine waste volume at reclaimed mine sites.

Keywords: Uranium; abandoned mines; reclaimed mines; Landsat; lidar; Time series; Google Earth Engine

Introduction

Oil companies discovered uranium in 1954 in the Texas Coastal Plain near Tordilla Hill (a site within Karnes County – Figure 1) [1], and mining began in 1959 [2]. The Texas coastal region is one of the three primary uranium mining regions in the United States [3]. Open-pit uranium mining began with shallow surface outcrop deposits, and deeper subcrop deposits were developed in the

 doi:10.20944/preprints202407.2426.v1

mid-1960s [1]. Uranium mining activity peaked during the energy crises of the 1970s and declined beginning in 1979 after a drop in economic demand [2]. The region produced an estimated 80 million tons of uranium, comprising 8% of the total national production [1]. The Texas Surface Mining and Reclamation Act went into effect in 1975 and the Federal Surface Mining Control and Reclamation Act of 1977 respectively established State and national uranium mine reclamation standards, as well as the Abandoned Mine Land Reclamation Fund. The Railroad Commission of Texas (RRC) has and continues to reclaim these mine sites, transforming the land use into agricultural row crop and pasture lands, alongside other types of land uses for energy development (e.g., oil and gas), such as in the region for petroleum production from the Eagle Ford Shale.

Although extensive records documenting the location and extent of mine pits and waste-rock piles, along with descriptions of reclamation activities are available for some mines, other mines were abandoned with little to no such documentation. The U.S. Department of Energy's U.S. Producing Uranium Mines database does not always track production to specific mines; therefore, the number and precise location of mine features are not always known [1]. The occurrence of undocumented mines is a global issue; basic knowledge of mine inventories and surveys is useful for studying environmental health risks and impacts [4]and evaluating the resource potential of mining and mine waste. According to the RRC, 23 known uranium mine pits were abandoned within Karnes, Atascosa, and Live Oak Counties prior to 1975 [2], though previous studies document a higher number [1,5]. Uranium production left a legacy of open-pit mining features such as pit craters and waste-rock piles which are still evident in modern-day digital topographic and remote sensing data [5].

Various lidar and multispectral data analysis techniques have been published for mine feature identification and characterization [6]. Multispectral imagery is available globally and commonly used for mine feature detection and monitoring [4]. Jing [7] demonstrated that diverse spectral band inputs, such as standard tasseled cap (TC) indices could be used to improve the detection of anthropogenic landscape disturbance related to mining and reclamation activities. Gitau et al. [8] used maximum likelihood classification to extract mine features where mine features are detectable from Sentinel 2 multispectral imagery. The Landsat archive provides more than 50+ years of image acquisition (1972–present). Cloud-hosted geoprocessing platforms (e.g., Google Earth Engine) efficiently process and render such immense data collections [9], thus enabling efficient temporal analysis of land cover/land use (LCLU) changes from mining activity and post-mining reclamation. Time-series analytical tools such as the LandTrendr algorithm, have been applied to study vegetation disturbance and track the progression of mining by plotting the normalized difference vegetation index across time [7].

For areas where mine features are not fully visible using optical spaceborne imagery, lidar laser scanning can be used to penetrate the vegetation canopy, extract topography, and identify anthropogenic features with high positional accuracy. The lidar point cloud and digital elevation models (DEMs) can be used to derive mine feature geometries, including waste pile and excavation volumes [10]. Lidar can be used to identify artificially engineered drainage features and fluvial geomorphic erosion characters present on mine waste [10]. Several geoprocessing toolsets are available to estimate mine feature volume, including the GlobalMapper Cut and Fill tool [11] which we applied in this study to characterize mine waste. Elevation data also can be used to track changes in the geomorphology of mining and post-mining LCLU when multiple timesteps are available [10]. Historical elevation data are rare and multiple lidar acquisitions for the same locations are expensive to produce. Therefore, we augment lidar analysis with multispectral data analyzed across extended periods of time.

In order to develop indicators defining legitimate mine features and areas of mining disturbance, our strategy was to investigate known mine sites within the study area and test remote sensing techniques that could be used to reveal similar features in other parts of the study area. The lidar 3-D elevation point cloud and derivatives such as the bare earth elevation surface, slope, topographic contours, and hydrography are indicative of mine feature geometry and texture. Time-lapse visual interpretation, and time-series spectral vectors using the Landsat multispectral imagery helped

 doi:10.20944/preprints202407.2426.v1

interpret historical areas of disturbance and the reclamation event sequence representing LCLU change and/or continuity.

This paper documents a mapping system developed to identify mine features and associated areas of disturbance and classify them into four categories: (1) abandoned mine pits (dry and water-containing), (2) abandoned waste-rock piles, (3) reclaimed mine pits (dry and water-containing), and (4) reclaimed waste-rock piles. Published mine site survey information, as well as descriptive mining and reclamation activity details provided by the Texas Railroad Commission and subsequent publications [1,2,12] are used as a source of ground-truth information and as a means of method validation. Secondly, we estimate mine feature volume from lidar-derived bare earth elevation. For mines where historical elevation data are available, we derive mine volumes by comparing geomorphic change before and after mining. The two mine volume estimation approaches were compared to examine potential sources of uncertainty.

Materials and Methods

2.1. Study Area

The study area is located in the south Texas Coastal Plain region, and is 11.5 km wide by 19.5 km long, at the intersection of Karnes, Atascosa, and Live Oak Counties (Figure 1). Much of the bedrock exposed and mined within the study area consists of sedimentary rocks from the Eocene Jackson Group, which is geologically the oldest Gulf Coastal Plain sedimentary unit from which uranium has been mined [3]. It consists predominantly of quartzo-feldspathic sandstone, mudstone, claystone and lignite members, the origins of which are coastal strandplain/barrier bar sand bodies, as well as lagoonal mud and swamp deposits, minor landward fluvial channel sand bodies and gulfward shelf-related mud deposits [13,14]. The overlying Oligocene to Miocene Catahoula Formation is believed to be the main source of much of the uranium mined in the area, in that the formation has been heavily leached of uranium by oxidizing and alkaline groundwaters. The uranium was then deposited as uranium "roll fronts" along reducing zones surrounded by impermeable barriers. Some of these uranium "roll front" ore zones are contained within the Catahoula Formation itself, as well as the underlying Jackson Group and overlying Oakville Sandstone of the Fleming Group and Goliad Formation (Figure 2) [1,3,15,16].

Approximately 55% of our study area is covered by shrub/scrub vegetation types according to the U.S. Geological Survey (USGS) National Landcover Dataset [17], while 32% is covered by hay and pastureland, and around 7% is covered by cultivated crops. One quarter of artificially planted and/or fallow vegetation types is considered pastureland, while hay, oats, corn, and cotton are the most common crop types according to the Texas Cropland Data Layer [18]. Native shrubland vegetation and related canopy are dominated by honey mesquite (*Prosopis glandulosa*), with understory of mixed bermudagrass (*Cynodon dactylon*), huisache (*Vachellia farnesiana*), granjeno (*Celtis pallida*), blackrush (*Vachellia rigidula*), buffelgrass (*Cenchrus ciliaris*), and lotebush (*Ziziphus obtusifolia*).

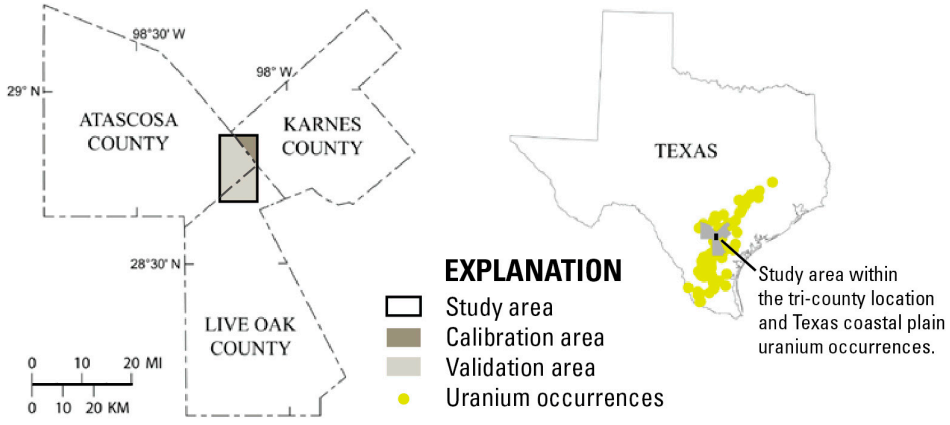

 doi:10.20944/preprints202407.2426.v1

Figure 1. Study area at the intersection of Karnes, Atascosa, and Live Oak Counties within the coastal plain uranium mining region of Texas.

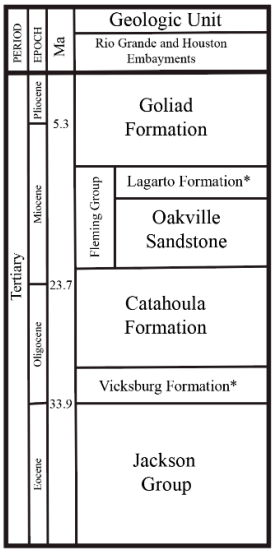

Figure 2. Study area stratigraphy modified from Hall et al., 2017[1] (*denotes units not discussed in the text, and are shown for stratigraphic context).

2.2. Uranium Mine Site and Reclamation Procedure Description

The first uranium discovered in Karnes County was mined at the Boso-Hackney Mine from an exposed outcrop where uranium-bearing chalk was present on the surface. The 1970s-era hard rock mining operations extracted bands of ore from often water-bearing subsurface units, which required deeper excavation. The deep mine pits, typically 27–91 m in depth, often filled with the seeping groundwater to produce pit lakes [12]. These open-pit mine walls were near vertical and were accompanied by nearby waste piles that were approximately 6–24 m high and had steep slopes. The RRC mapped mine sites using aerial surveys [12] and published reclamation activities at those sites [2]. These data include mine name, location, reclamation status, reclamation procedures and dates of reclamation activities that were conducted at individual mine sites. Hall et al. [1] published comprehensive research on the Texas Coastal Plain geology, uranium production history including known, currently active, and no longer producing mines, and potentially undiscovered resources [1,19].

For this study, the size, depth, excavation method, and timeline of uranium mining activity were used to help differentiate the uranium mines from other excavations, such as lignite mines and industrial rock, sand, and gravel quarries. Oil and gas drill pads are very common features in this region, related to production from the underlying Eagle Ford Shale [20]. Lignite surface mining operations within the Jackson Group commenced in Atascosa County in 1980. Thin benches (approximately 1 m thick) of lignite were extracted from these mines utilizing dragline excavation methods to remove approximately 30 m of overburden. There is presently one active coal mine in the tri-county region, the San Miguel mine [21], which is located just outside of the study area outlined in Figure 1 [22].

Unstable and steep uranium pit walls and waste pile slopes containing radioactive materials posed health and safety hazards, and deterioration of water quality from sedimentation, metals, salinity, and acidification justified reclamation of these sites [2]. According to the Railroad Commission of Texas [2], the reclamation strategy for open-pit uranium mines is to first drain the mine pits of water, then apply standard earthwork procedures to reduce slope of the mine features, followed by revegetation of slopes to manage soil erosion and to maintain the integrity of the earthwork effort. The earthwork processes include salvaging the topsoil, burial of radioactive and

 doi:10.20944/preprints202407.2426.v1

acidic material, flattening of pit and pile walls, addition of topsoil, construction of overland flow drainage canals, and wind and water erosion control. The revegetation process starts with planting a temporary rapidly growing cover crop, followed by the establishment of a permanent grass species [2,23]. The study area was selected for analysis because of the existing variety of overlapping remote sensing datasets including temporally continuous Landsat imagery and lidar data acquired over all three counties. Additionally, advanced multispectral and hyperspectral analyses for uranium-bearing minerals were published for the study area [5,24], and documented mine inventories and reclamation procedures [1,2,12] were available and could be used for interpretation, calibration, and validation.

2.3. Lidar 3-D Elevation Analysis of Mine Features and Derivative Data Products

The lidar high density 3-D elevation point clouds used in this study were produced from airborne laser scanning in the near-infrared (NIR) spectra. Elevation is determined by the time of the laser reflection return traveling at the speed of light. Each laser return is attributed with high-precision geospatial coordinates (x, y) and elevation (z) values, such that the culmination of returns delivers a point cloud (Figure 3). Laser scanning penetrates the vegetation and reveals vegetation canopy structure, topography, and anthropogenic features present on the landscape such as excavations, above-ground structures, and infrastructure (Figure 3). Lidar-derived bare earth DEM, slope, elevation contours, and hydrography were produced as analytical products for this study to explore, identify, and differentiate mine features (Figures 3 and 4) using Global Mapper desktop software.

Two lidar acquisitions were used in this analysis, both acquired at different times over different but overlapping areas. These lidar data were produced by USGS 3-D Elevation (3DEP) program in collaboration with local stakeholders and reviewed by the USGS to meet data quality and lidar point cloud classification standards. At the time of this study, these were the best available and the only two lidar data coverages published in the public domain for the study area. Both datasets were combined seamlessly using the overlapping area of coverage. A 50 cm nominal point spacing spatial resolution point cloud acquired in 2013 was used to explore Karnes County. The accuracy of that data was reported to have an overall RMSEz (Root Mean Square Error of the z direction) of 7.029 cm for bare earth returns [25]. A 70 cm nominal point spacing spatial resolution point cloud was acquired in 2018 for Atascosa and Live Oak Counties. The latter dataset has a reported RMSEz of 5.9 cm for checkpoints in non-vegetated terrain and was quality-assurance tested to meet a less than 10 cm vertical accuracy standard [26].

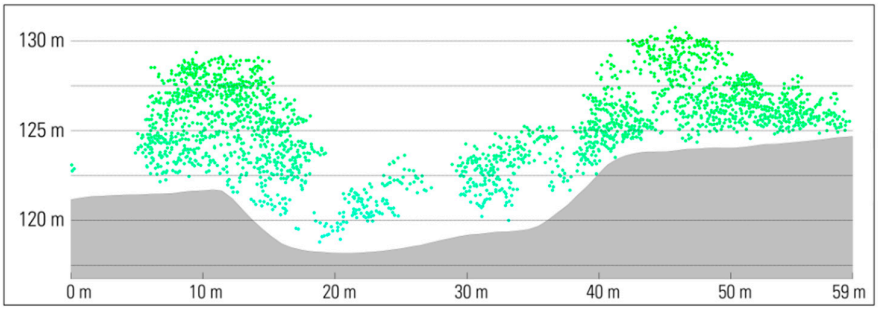

A

 doi:10.20944/preprints202407.2426.v1

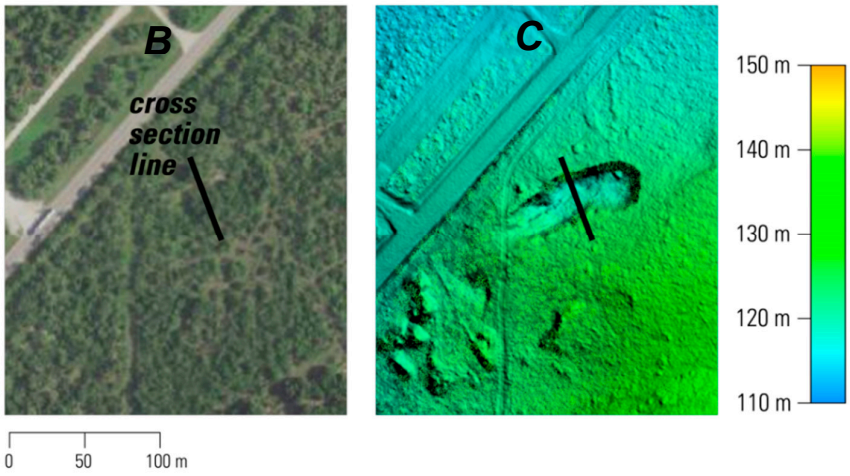

Figure 3. The lidar point cloud cross section (A) reveals the Boso-Hackney mine pit from underneath vegetation cover otherwise not apparent in (B) multispectral imagery true-color visualization. The bare earth elevation surface (C) is extracted from the lidar point cloud.

2.4. Bare Earth Topography

Lidar laser scanning penetrates the vegetation canopy to measure the bare earth surface topographic elevation and often reveals anthropogenic modifications to the landscape such as mine excavation pits and waste pile features, and areas that were disturbed by mining operations (Figure 3). Bare earth DEMs were derived from pre-classified ground returns using the Global Mapper Create Elevation Grid tool. All non-terrain surface features present on the landscape (e.g., buildings and vegetation) were removed when generating the final DEM. The bare earth DEMs (e.g., Figure 3) were generated at the same spatial resolution as their original lidar point cloud. Radiation at NIR wavelengths is absorbed by water, therefore the absence of lidar ground returns is a useful indicator of the presence of surface water. Gaps in ground returns were intentionally retained after interpolation of the DEM surface to reveal pit lake features (Figure 5). Mine feature geometry and volumes were derived using this bare earth DEM data. The resulting lidar bare earth DEM products and the detailed processing steps are documented and published in a USGS Data Release [27]. Topographic contour vectors were derived from the bare earth DEM and calculated at 5 m intervals using the Global Mapper Create Contours tool. Topographic contours helped aid in qualitative visual interpretation, thereby further helping us in identifying and differentiating between reclaimed and abandoned mine features (Figure 4C).

2.5. Slope

Slope was generated from the bare earth DEM data using the ESRI Slope tool where steepness of the land surface is calculated using a 3x3 pixel window. Threshold values were grouped into 2 classes based on visual interpretation and values reported by the Railroad Commission of Texas [2,12]. These classes were selected to help differentiate abandoned and reclaimed mine pits and waste piles from other natural and anthropogenic features on the landscape. The Gulf Coastal Plain region is observed to contain predominantly gradual slopes less than or equal to 5°, gently dipping towards the Gulf of Mexico. The RRC reported that the reclamation procedures implemented engineered pit and pile walls to have reduced steepness for safety and to control erosion [2]. We observed that slopes greater than 5° but less than 14° reveal reclaimed mine pit and pile features. Slopes greater than 20° reveal severe erosion features and steeper wall slopes present at “unreclaimed” or “partially reclaimed” pit excavations and waste piles in the study area, which is consistent with the mine pit and pile slopes reported by the Railroad Commission of Texas [12] (Figure 4B). Other natural and anthropogenic features can exhibit such ranges of slopes on the landscape, such as escarpments observed at Tordilla Hill and fluvial stream channels. However, those features are not numerous

 doi:10.20944/preprints202407.2426.v1

within our study area. The slope classes we derive can be considered generalized and simplified for this study.

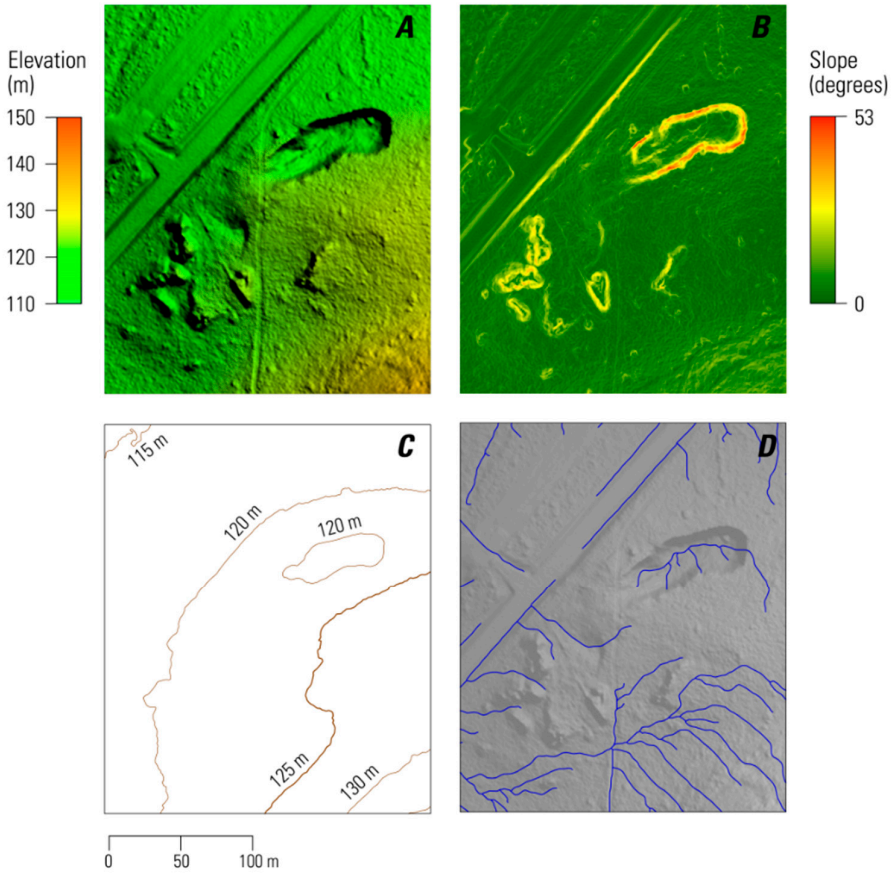

Figure 4. Lidar derivative products generated at the Boso-Hackney mine site: A. bare earth elevation, B. slope, C. elevation contours, D. hydrographic stream vectors.

2.6. Hydrography

The approach for deriving stream hydrography from DEMs produces three datasets: first, fill depressions (i.e., sinks) in the DEM; next, flow direction; and finally a flow accumulation dataset is produced [28] to be vectorized into a stream network representing the surface hydrology overland flow pattern (Figure 4D). For this study, the Global Mapper Create Watershed tool was used to generate such watershed analysis. The first step in the conventional process is to fill depressions to force connectivity of stream vectors; however, because our goal is to reveal hydrographic sinks (i.e., mine pits), we reduced the depth threshold for the sinks to 0.2 m so that the resulting stream vectors are intentionally segmented. Disruptions in the stream vector continuity produced with adjusted sink depth threshold values help reveal mine- or quarry-related features and areas of mine disturbance in the study area (Figure 4D).

Mine features in our study area have distinct hydrographic characteristics which aid in their visual interpretation. Natural stream vectors tend to create branching patterns as tributaries converge and accumulate on the gentle sloping Gulf Coastal Plain landscape. Reclaimed mine features have engineered water channels needed to manage erosion. Therefore, hydrography helps reveal such artificially engineered features, as well as erosion features (e.g., gullies) on unreclaimed mine pits and waste piles. Surface water lakes and ponds in the study area are also observed to be of anthropogenic origin. Stream impoundments have a clear connectivity with natural hydrographic patterns. For example, features such as ponds developed for watering livestock are created by constructing earthen dams that intercept naturally occurring streams. In contrast, the extraction of

 doi:10.20944/preprints202407.2426.v1

uranium ore from the groundwater-saturated lithologic members often results in excavation pits filling with groundwater, thus creating pit lakes. These water bodies do not follow natural surface hydrography patterns in the study area and disrupt the observed natural hydrography. Shallow pits mined at surface outcrops (i.e., the Boso-Hackney mine) do not appear to have been excavated to the depth that would tap groundwater and, therefore, shallow dry pits are also present as well – these excavations can potentially hold ephemeral pools that trap surface water runoff from precipitation events.

2.7. Texture

Use of the high spatial resolution bare earth DEM and slope data reveals topographic textures. The reclaimed features display a smooth surface texture created by re-engineered slopes during the earthwork phase of reclamation (Figure 5). Rough texture and steep slopes (i.e., slope greater than 80°) together identify areas of erosion, resolving erosion gullies that are present on the abandoned mine features (Figure 5). Texture was visually interpreted to classify mine features as either reclaimed or abandoned.

 doi:10.20944/preprints202407.2426.v1

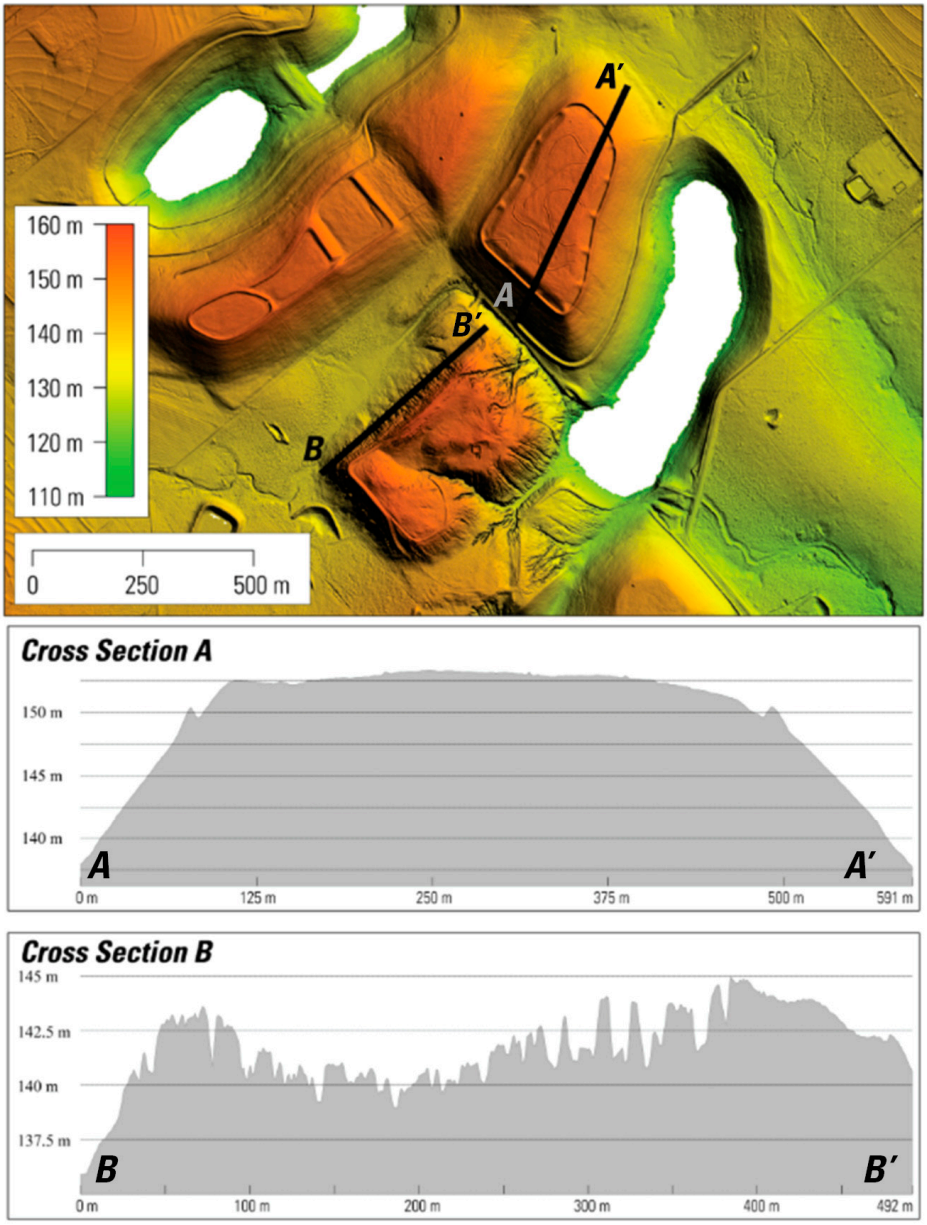

 doi:10.20944/preprints202407.2426.v1

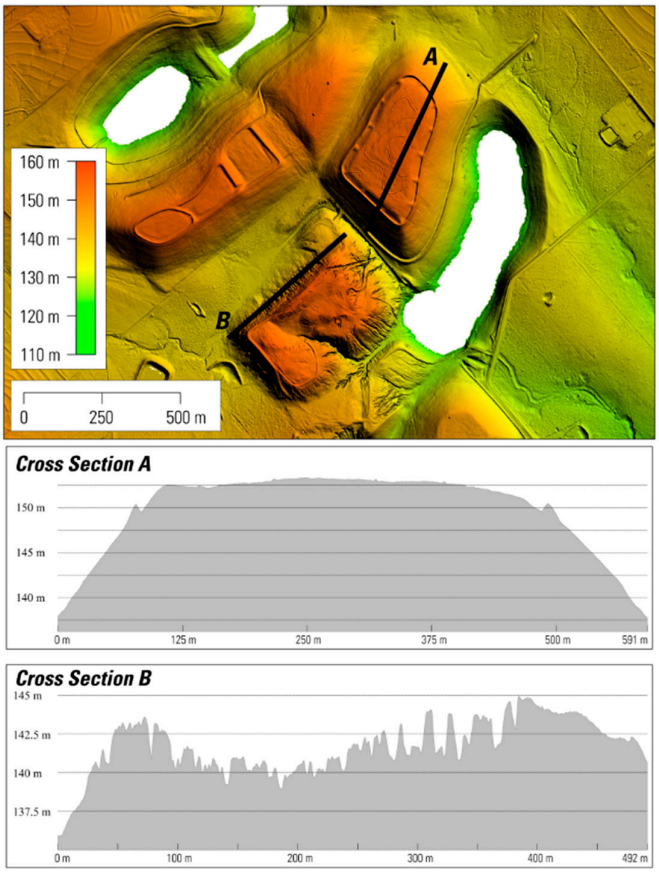

Figure 5. Cross section A presents a consistent smooth texture across the reclaimed mine pile; in contrast, cross section B provides an example of erosion features present on the slope of an unreclaimed mine pile.

2.8. Temporal Analysis of Mine Lifecycle

Temporal analysis was used to explore the life-cycle of mining and to provide evidence for reclamation activity. Temporal analysis included both quantitative time-series and qualitative time-lapse image interpretation. Notably, we used these two approaches in tandem to support the interpretation of the LCLU change for the mining areas, which included the presence or absence of an actual reclamation temporal sequence signal in and around mine features.

Google Earth Engine (GEE) enables us to efficiently render imagery, filter and screen them for suitable cloud conditions and image quality, and to visualize and iterate both seasonally and annually through the cloud- hosted Landsat archives, from 1972 to present. GEE was also used to generate rapid quantitative results, which included spectral vector time-series plots representing LCLU change or continuity over time. Both qualitative time-lapse analysis and quantitative spectral-based time-series analysis are explained in further detail below.

2.9. Qualitative Time-Lapse Interpretation

The temporal life-cycle of mining activities starts with land disturbance (Figure 6A), then progresses into the appearance of distinct mine pit and pile features (Figure 6B). The latter may be followed by either the reclamation activities described in Section 2.2 (Figure 6C), or by abandoned mine features remaining on the landscape. Distinguishing characteristics left behind during the latter stage include readily identifiable features such as exposed bare earth with severe erosion features, which are amenable to detection using spectral remote sensing methods [5,24]. These mine pit and

 doi:10.20944/preprints202407.2426.v1

waste pile features are notably present in clusters, where reclaimed and abandon features often coexist adjacent to one another, especially those within the Karnes County portion of the study area.

We used the imagery to visually inspect for mining activity, by starting to examine images taken by Landsat 1 in the summer of 1972. For the Landsat 1 through Landsat 4 sensors, 60 m spatial resolution and Tier 2 data quality were used when Tier 1 data were not available. With the introduction of Landsat 5 in 1984, 30 m spatial resolution Tier 1 surface reflectance was consistently available for time-lapse analysis. The 30 to 60 m spatial resolution effectively captures the shape and spatial extent of mining features used in both our time-lapse visual interpretation and spectral-based quantitative time-series analysis.

The GEE user interface was used to filter the Landsat archive and select the imagery that best revealed the progression of mining activities with minimal cloud cover. Imagery was visualized by generating false-color infrared composite where the near-infrared, red and green wavelength channels are displayed as red, green and blue, respectively. These images were used to visually interpret surface features including vegetation (which appears red – Figure 6A-D), water, and exposed bare earth (which appears white, e.g., Figure 6C). Visual/ interpretation elements of color pattern, texture, shape, and size were reviewed to follow the progression of mining through the decades as illustrated in Figure 6A-D. Mining was most active in the study area in the early 1970s [12].

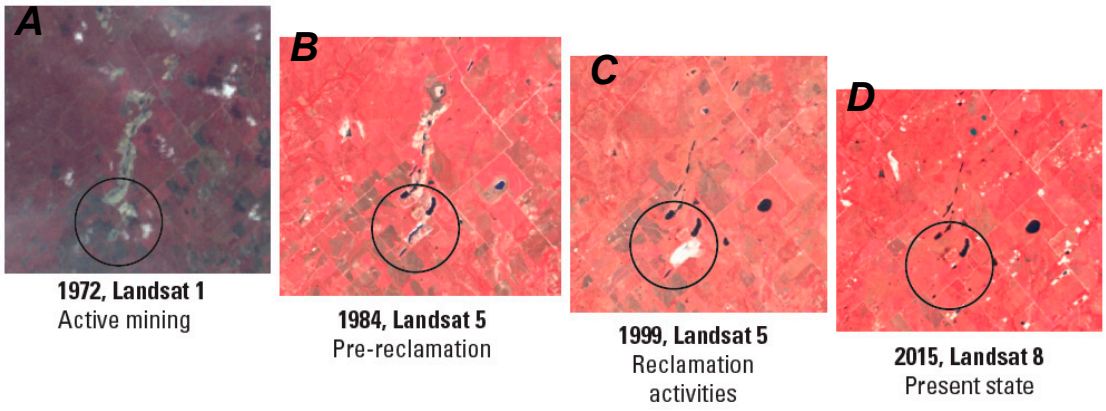

Figure 6. Landsat multispectral imagery time-lapse revealing LCLU changes associated with mining activities, 1972-2015: A. active mining, B. pre-reclamation, C. reclamation activities, and E. post-reclamation land cover.

2.10. Quantitative Time-Series Analysis

The LandTrendr Pixel Time Series Plotter user interface of GEE was used to graphically plot surface reflectance values indicative of LCLU across time. The algorithm calculates a median spectral value from the summer season and plots one value per year. A temporal break-point in the spectral vector is representative of a land cover change event. In contrast, a continuous flat-line-shaped spectral vector is indicative of no change ([29] and references included therein). For a single 30 x 30 m pixel in the surface reflectance calibrated Landsat thematic mapper (TM) archive (1984 - present), the LandTrendr algorithm in Google Earth Engine (LT-GEE) extracts and plots various spectral indices that produce spectral vectors representative of either LCLU change or continuity [29](Figure 7). The LT-GEE tool uses Landsat 5 through Landsat 8 imagery; therefore, it analyzes surface features present on the landscape between 1984 and present.

Tasseled Cap Transformation spectral indices were selected to reveal trends of LCLU type at the spatial scale of a single 30 m Landsat pixel over time as follows: (1) Tasseled Cap Wetness (TCW), (2) Tasseled Cap Brightness (TCB), and (3) Tasseled Cap Greenness (TCG) [30]. High TCW values represent surface water while lower values represent varying degrees of soil moisture. TCB

 doi:10.20944/preprints202407.2426.v1

represents brightness of bare soils as a function of various factors including mineralogy, moisture, and organic matter content. TCG values represent the presence of photosynthetic biomass. With respect to the life-cycle of mining activities, reclamation is revealed by shifts in these spectral vectors (Figure 7A), whereas continuous spectral vectors reveal the absence of reclamation events during the period of observation (Figure 7B). These results are summarized in section 3 and tables described therein and discussed further in section 4.3.

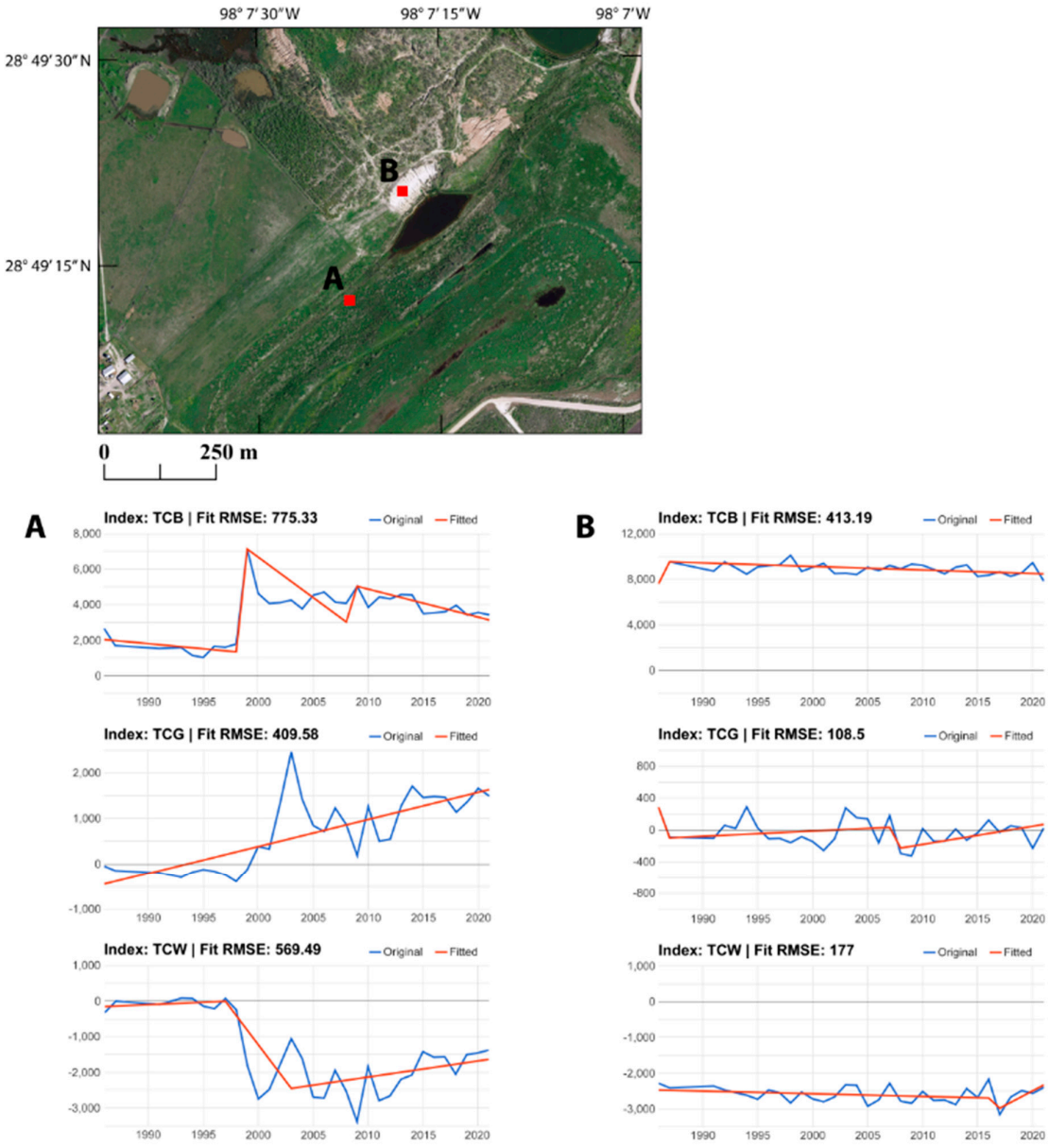

Figure 7. Time series comparing (A) shifts in spectral indices (Tasseled Cap Wetness, Tasseled Cap Brightness, and Tasseled Cap Greenness) indicative of the mine reclamation sequence (pit de-watering, earthwork, and re-vegetation), to (B) no change in spectral vectors over time, indicative of no change in LCLU for the time period analyzed at the mine sites.

2.11. Classification System of Mine Features

The goal of the "multiple lines of evidence" classification system design was to be able to uniquely distinguish individual classes. For each mine site in the Karnes County calibration area

 doi:10.20944/preprints202407.2426.v1

(Figure 1), the geospatial data derived from the lidar point cloud (i.e., bare earth, topographic texture and contours, hydrography, and slope) were used in combination with the temporal analysis (i.e., time-series and time-lapse image interpretation) to identify mine features, and to determine if a feature underwent reclamation, or was abandoned based on the unique parameters outlined in the classification system shown in Table 1. The data thresholds used to differentiate classes were selected based on reported thresholds described in previous sections (e.g., slope thresholds) and further interpreted based on manual sensitivity of the geospatial data layers' ability to be used individually and collectively to uniquely capture the respective mine feature classes. The interpretation of the areas of disturbance relied heavily on the bare earth textures surrounding mine features and documented mines. Mine name labels were assigned based on published point locations [1,2,12].

Table 1. Mine classification system designed to uniquely identify and differentiate abandoned and reclaimed mine pit and pile features.

I. Abandoned Mine Pit
1. Pit feature present in bare earth elevation - reported size 27–91 m depth, with potential presence of water within pit.
a. Pit drainage supported by hydrography (Figure 4D).
b. Pit elevation change supported by elevation contours (Figure 4C).
2. Slope steepness greater than or equal to 20° (Figure 4B).
3. Presence of erosion gullies and rough texture on bare earth surface (Figure 5B).
a. Interpretation of erosion features supported by hydrography (Figure 4D) and steep slope.
4. Time-lapse: visual interpretation revealing mining activities with no evidence of reclamation (Figure 6).
5. Time-series: continuity of spectral vectors with no evidence of the reclamation sequence (Figure 7B).
II. Abandoned Mine Waste Pile
1. Waste pile feature present in bare earth elevation - reported size 6–24 m.
a. Waste pile elevation change supported by elevation contours (Figure 4C).
2. Slope steepness greater than or equal to 20° (Figure 4B).
3. Presence of erosion gullies and rough texture on bare earth surface (Figure 5B).
a. Interpretation of erosion features supported by hydrography (Figure 4D) and steep slope..
4. Time-lapse: visual interpretation revealing mining activities with no evidence of reclamation activities (Figure 6).
5. Time-series: continuity of spectral vectors with no evidence of the reclamation sequence (Figure 7B).
III. Reclaimed Mine Pit
1. Pit feature present in bare earth elevation - reported size 27–91 m depth, with potential presence of water within pit.
a. Pit drainage supported by hydrography (Figure 4D).
b. Pit elevation change supported by elevation contours (Figure 4C).
2. Slope greater than 5° and less than 14° (Figure 4B).
3. Presence of smooth texture of engineered resurfacing and water drainage systems on bare earth surface (Figure 5A).
a. Interpretation of pit drainage supported by hydrography (Figure 4D).
4. Time-lapse: visual interpretation revealing mining activities (Figure 6C).
5. Time-series: breaks in spectral vectors representing the reclamation sequence of de-watering, earthwork, and revegetation (Figure 7A).
IV. Reclaimed Mine Waste Pile
1. Waste pile feature present in bare earth elevation - reported size 6–24 m.
b. Waste pile elevation change supported by elevation contours (Figure 4C).
2. Slope greater than 5° and less than 14° (Figure 4B).
3. Presence of smooth texture of engineered resurfacing and water drainage systems on bare earth surface (Figure 5A).
a. Interpretation of pile drainage supported by hydrography (Figure 4D).
4. Time-lapse: visual interpretation revealing mining activities (Figure 6C).
5. Time-series: breaks in spectral vectors representing the reclamation sequence of de-watering, earthwork, and revegetation (Figure 7A).

2.12. Method Evaluation

In order to validate our methodology, we divided our study area into a calibration area (Karnes County) and a blind validation portion for the remainder of the study area (Atascosa and Live Oak Counties) (Figure 1). Karnes County was chosen because of the known and documented mines in this county as discussed in previous sections. We used well documented information from mine sites in the calibration area to develop our classification system. This system was then applied towards identifying abandoned and reclaimed mine features in the validation area. The total surface areas of associated mine disturbance features were delineated to create vectorized "mine feature extent" maps (Figure 8), which are also available digitally as a USGS Data Release [27].

Notably, the location and number of mines in Atascosa and Live Oak counties were not reviewed in advance, and therefore the validation portion of the study area served as an area of "blind analysis." The goal of the blind validation was to assess the success of the classification system with the intent of iteratively refining our classification approach.

 doi:10.20944/preprints202407.2426.v1

2.13. Mine Volume Estimation

Mine areas of disturbance were used to quantify the volume of waste-rock piles and pits. We explored two methods for deriving mine feature volume: (1) for all mines, we used the Global Mapper Cut and Fill tool [11] to estimate volume from the post-mining lidar-derived bare earth topography, and (2) where historical pre-mining USGS National Elevation Dataset (NED) DEM topographic data were available for a subset of mines, we quantified volume by taking the geomorphic difference between pre- and post-mining topographic surfaces as discussed below. Bathymetric data for pit lakes were unavailable, therefore mine pits were eliminated from volume analysis if the presence of water was detected. Because verified waste-rock pile surveys were unavailable and their base elevations were unknown, both methods were expected to over- or under-estimate feature volumes. A simple comparison of these two volume estimation approaches was conducted to gauge outcomes and to help identify and describe limitations.

Pit and rock pile volumes were calculated using the Cut and Fill tool to estimate the total volume for all mines identified in this study. Terrain above the mine feature base height was calculated as pile volume, and any terrain below the mine feature base height was used to calculate the pit volume. The Cut and Fill tool interpolates a flat planar surface in the space between elevation points sampled from the mine feature polygon to then 'cut' a base height from which pit and pile volumes are estimated.

Where historical DEM data represented the pre-mining terrain topography, these data were utilized to capture the complexity of natural depressions or rises in landscape geometry, in our hope to advance volume estimations beyond the simplified flat planar surface interpolated by the Cut and Fill tool. These data were obtained from the USGS NED [31]. The 1/3 arc-second (approximately 10 m) spatial resolution NED DEM revealed historical pre-mining land surface elevations at 4 of the 14 documented mines in the study area. The NED DEM was resampled to the 50 cm spatial resolution to be consistent with and to retain the native spatial resolution of the 2013 lidar-derived bare earth DEM using bilinear resampling. Volume estimates were calculated for the mine feature extents by taking the geomorphic difference between the historical pre-mining resampled NED DEM and the lidar-derived bare earth post-mining topography.

Results

Table 2 summarizes the results of applying the classification system (Table 1) to known mine pit and waste pile sites compared to published ground truth information from RRC [2,12] and Hall et al. [1]. Our ability to identify mine sites as either reclaimed or unreclaimed yielded consistent results when compared to the published data.

Fourteen mine pit and/or waste pile sites were documented and mapped in the study area – where mine pit and pile features covered an area of 496 hectares, and the total area of disturbance was 649 hectares (Table 3). The calibration area contained 11 uranium mines. The blind validation area revealed 3 additional uranium mines, all of which were known mines after applying our classification approach (Table 1). Of the 14 mines in the study area, 12 were documented as reclaimed. Two mines were classified as unreclaimed: (1) the McCrady waste pile, which was documented by the RRC as unreclaimed and (2) the Boso-Hackney mine which was documented as partially reclaimed (Table 2). Fourteen mine pits were observed, where two of the mine pits were dry. Volume was estimated for these two dry pits (579,717 m^3) using the Cut and Fill approach. Of the 14 documented mines, 21 waste-rock piles were detected and resulted in the total volume of 20 million m^3 (Table 3) using the Cut and Fill approach.

Historical pre-mining terrain data were available at four of the 14 documented mines: the Butler pit and piles, Kellner piles, Weddington-north piles, and the Weddington-Susquehana piles (Table 3). When we compared the total volume estimate for these four mines, the Cut and Fill tool consistently calculated less volume compared to the historical DEM-derived volumes (-21%) (Table 3).

 doi:10.20944/preprints202407.2426.v1

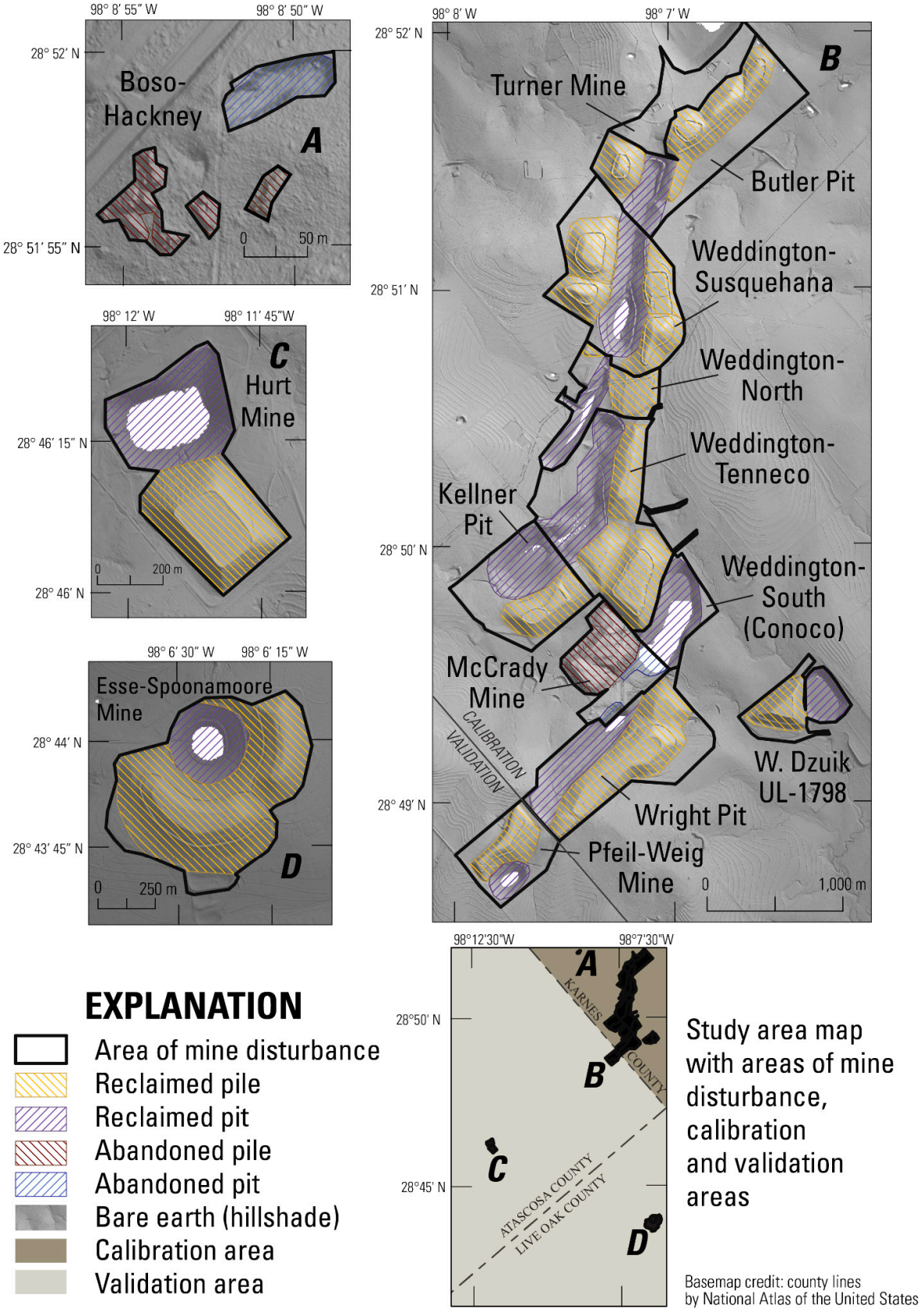

 doi:10.20944/preprints202407.2426.v1

Figure 8. Mine site maps with classified abandoned and reclaimed mine features and areas of mining disturbance.

Table 2. Results of the spatiotemporal classification system for the identification of reclaimed and unreclaimed mine features and areas of disturbance associated with mines located in the calibration and validation areas. The table also presents the results of observed slope, and time-series analysis for each mine, and compares observations to published reports of reclamation status and timeline (*[12] , ^^[2], ^[1]).

Name	Lidar analysis				Time series analysis				
	Calibration /Validation	Reported reclamation^^	Observed reclamation	Observed slope	Observed pit de-watering	Reported earthwork^^	Observed earthwork	Reported re-vegetation^^	Observed re-vegetation
Boso-Hackney*^	Calibration	Partial	No	≥20°	non-detect	unknown	non-detect	unknown	non-detect
Butler Pit*^	Calibration	Yes	Yes	≤14°	1994	1995	1994	1996	1996
Kellner Pit*^	Calibration	Yes	Yes	≤14°	2001	unknown	2001	unknown	non-detect
W. Dzuik UL-1798*^	Calibration	Yes	Yes	≤14°	Prior to 1984	unknown	Prior to 1984	1985	non-detect
Weddington-North*^	Calibration	Yes	Yes	≤14°	2011	unknown	2011	unknown	2013
Wright Pit*^	Calibration	Yes	Yes	≤14°	1999	1998	1999	1999	2003
Weddington-South (Conoco)*^	Calibration	Yes	Yes	≤14°	1998	2000	1998	unknown	1999
Turner Mine*	Calibration	Yes	Yes	≤14°	Prior to 1984	unknown	Prior to 1984	unknown	non-detect
Weddington-Susquehana*^	Calibration	Yes	Yes	≤14°	1996	1997	1996	1997	1997
Weddington-Tenneco*^	Calibration	Yes	Yes	≤14°	1997	1997	1997/1998	1999	1999
McCrady Mine*^	Calibration	No	No	≥20°	non-detect	unknown	non-detect	unknown	non-detect
Esse-Spoonamoore Mine*	Validation	Yes	Yes	≤14°	2004	unknown	2004	unknown	2007
Hurt Mine^	Validation	Yes	Yes	≤14°	Prior to 1984	unknown	Prior to 1984	unknown	Prior to 1984
Pfeil-Weig Mine^	Validation	Partial*	Yes	≤14°	2002	unknown	2002/2003	unknown	2007

Table 3. Areas of mine disturbance, areas of mine features, and mine feature volumes calculated by lidar- derived bare earth Cut and Fill analysis, compared to volumes calculated for the lidar-derived bare earth and the NED DEM pre-mining geomorphic difference (for a sub-set of mines indicated by bold font). 'N/A' represents areas where volumes were not estimated because water was present in mine pits or piles that were not detected within a reclaimed mine area of disturbance. Information was left blank if NED DEM data were not available for mine sites (*[12]; ^[1]).

Name	Area of disturbance, ha	Area of pit and pile features, ha	Global Mapper volume estimates				Pre-mining NED DEM volume estimates				Percent difference in pit volume (Global Mapper - NED DEM)	Percent difference in pile volume (Global Mapper - NED DEM)
			Pit volume, m^3	Pit count	Pile volume, m^3	Pile count	Pit volume, m^3	Pit count	Pile volume, m^3	Pile count		
Boso-Hackney^*	0.7	0.6	6,562	1	1,788	3	---	---	---	---	---	---
Butler Pit*^	**81.58**	**55.5**	**573,155**	**1**	**2,657,582**	**2**	**343,071**	**1**	**3,463,797**	**2**	**50%**	**-26%**
Kellner Pit^*	53.6	39.3	N/A	1	1,115,409	1	---	---	---	---	---	---
W. Dzuik UL-1798^*	27.5	21.5	N/A	1	956,905	1	---	---	---	---	---	---
Weddington-North*^	**31.1**	**25.9**	**N/A**	**1**	**156,016**	**2**	**N/A**	**N/A**	**249,949**	**2**	**N/A**	**-46%**
Wright Pit^*	76.8	64.4	N/A	1	3,172,296	1	---	---	---	---	---	---
Weddington-South (Conoco)^*	25.5	21.1	N/A	1	N/A	0	---	---	---	---	---	---
*Turner Mine**	28.4	N/A	N/A	0	N/A	0	---	---	---	---	---	---
Weddington-Susquehana*^	**85.6**	**72.8**	**N/A**	**1**	**2,429,090**	**4**	**N/A**	**N/A**	**2,873,336**	**4**	**N/A**	**-17%**
Weddington-Tenneco*^	**96.2**	**77.5**	**N/A**	**1**	**3,027,381**	**3**	**N/A**	**N/A**	**3,656,933**	**3**	**N/A**	**-19%**
McCrady Mine^*	36.7	28.3	N/A	2	2,088,562	1	---	---	---	---	---	---
*Esse-Spoonamore Mine**	52.6	49.0	N/A	1	3,018,777	1	---	---	---	---	---	---
*Hurt Mine^*	52.8	21.4	N/A	1	858,072	1	---	---	---	---	---	---
Pfeil-Weig Mine	31.7	18.4	N/A	1	630,985	1	---	---	---	---	---	---
Totals for all mines												
Sum - all mines	681	496	579,717	14	20,112,863	21						
Mean - all mine features	49	38	41,408	1	957,755	1.5						
Totals for mines where pre-mining NED DEMs were available for comparison to post-mining DEMs												
Sum	**295**	**232**	**573,155**	**4**	**8,270,069**	**11**	**343,071**	**1**	**10,244,015**	**11**	**50%**	**-21%**
Mean - per mine feature	**74**	**58**	**573,155**	**1**	**751,824**	**2.8**	**343,071**	**1**	**931,274**	**2.8**	**50%**	**-21%**

Summary and Discussion

4.1. Classification and Multiple Lines of Evidence Strengths and Limitations

The RRC [2,12] and Hall et al. [1] provide useful information such as mine site locations, mine feature characteristics, and reclamation timelines; however, the published information is limited for some data parameters that we were able to successfully derive from remote sensing techniques. Although the validation area is geographically larger than the calibration area (Figure 1), the outcome of the blind validation assessment revealed three additional uranium mines. Future work could benefit by expanding the study area to include even more mines for such validation assessment. As

 doi:10.20944/preprints202407.2426.v1

such, our spatiotemporal approach using multiple lines of evidence (bare earth, topographic contours, hydrography, slope, and texture) combined with the temporal analysis (time-lapse false-NIR image interpretation, and TCB, TCW, and TCG time-series) allowed for successful identification of relatively large uranium mine features and areas of mining disturbance. Additionally, we were able to differentiate features that underwent reclamation from those which were unreclaimed and subject to erosion. This includes mine features that do not appear to have undergone reclamation using standard procedures outlined by the RRC.

Lidar laser scanning allowed for detection of bare earth topography that would not always be visible to aerial and multispectral imagery alone where the features are covered with vegetation. Because the lidar data have high spatial resolution and vertical accuracy, many anthropogenic excavations are revealed in great detail. Bare earth elevation and slope served as the primary data that led to the identification of large uranium mine features. The large size and volume of these uranium mine features help to uniquely identify and differentiate them from smaller excavations such as prospect and gravel pits, aggregate quarries, and lignite mines also present in the study area. We concede that the Boso-Hackney Mine is elusive because its size and depth are similar to gravel pits observed in the study area, and because multispectral imaging would detect primarily vegetation (Figure 3). The Boso-Hackney is well documented because it is the first known mine in the region and is located in the calibration area, so it was initially used for the development of the mapping system; however, smaller, shallow, partially reclaimed, mines like the Boso-Hackney would need additional investigation and/or lines of evidence to eliminate false positives and false negatives. Because our methods focused on identifying uranium mine features based on structural, geometric, and temporal change factors derived from remote sensing data, we concede that we are unable to determine the presence or absence of uranium minerals at each mine site. For example, in addition to potential residual naturally occurring uranium, Brandt et al. [12] reported that the Boso-Hackney mine contains buried radioactive waste. Radiometric gamma radiation surveys [32] could help provide evidence that these smaller excavation features are uranium mines. Additionally, for mines with exposed lithologic features, the ability to verify the presence of either uranium or associated minerals at these mines would benefit from incorporating spectral reflectance data [5,24].

By combining bare earth texture data with time-lapse and time-series analyses, we are able to map areas of disturbance for reclaimed mines documented by the RRC as areas that experienced earthwork, in addition to the actual mine pit and pile features. Topographic contour and hydrography data provided vector layers which helped to support interpretation of such features. These supporting data layers helped to reduce false positives in our interpretations by assisting us in eliminating other anthropogenic features such as agricultural contour plowing, and earthen dams used to impound water ponds along streams.

The classification system was strengthened by augmenting lidar analysis with the temporal analysis. Time-lapse image analysis of the Landsat archive images reveals qualitative interpretation of landscape disturbances from mining activity, which is helpful for observing peak mining activities throughout the 1970s energy crisis era. Time-series analysis helped provide evidence for whether the disturbances were abandoned or reclaimed mine features (with the exception of the 'partially reclaimed' Boso-Hackney Mine which was reported to contain buried mine waste and concurrently met criteria for the abandoned/unreclaimed mine classes). The LandTrendr algorithm calculated TCB, TCW, and TCG spectral indices that were representative of land cover for point locations on an annual basis, which in the case of this study were constrained to the summer months [29]. Notably, any reclamation activities that occurred after the index was calculated for that preceding summer were revealed in the index calculation for the following year. This could be a factor that contributes to the explanation of an inconsistency with published dates by 1 year. The LT-GEE algorithm's TCG spectral index was not always able to detect a prominent revegetation event signal. The reasons why the TCG signal was not consistently detectable were beyond the scope of this work; however, it should be noted that remote sensing observations can be more reliable for capturing revegetation events on the landscape than ground surveys which are done intermittently with multiple years and sometimes decades intervening between updates. The LT-GEE algorithm is computationally efficient for analyzing LCLU across multiple decades, and time-series algorithms with greater temporal precision could be employed to resolve reclamation events and timelines in greater temporal detail,

 doi:10.20944/preprints202407.2426.v1

e.g., to explore seasonal variation of revegetation. The success of achieving successful revegetation could be driven by localized precipitation events, and/or regional climate variability. Also, the stability of vegetation cover can vary depending on whether native vegetation is replanted, or if the land will be used for row crops, grazing or pastureland [12,23]. Because the period of observation ranges from 1984 to present, the absence of observed reclamation sequence signals is not considered conclusive verification that a site was not reclaimed, as it is possible that reclamation activities could have occurred prior to the period of observation. For example, Boso-Hackney mining (1959) pre-dates the launch of Landsat 1. Our use of time-series and time-lapse imagery (Table 1) for observing temporal changes related to mining and reclamation activities proved less reliable by themselves, but the lidar and imagery datasets provide a reliable and complete summary of mining and reclamation activities across decades when the two datasets are coupled together. Despite the reliability and accuracy issues noted with the imagery, these data provided valuable LCLU change data not captured by the static lidar datasets. The data thresholds used to develop unique identifiers were designed to differentiate mine classes; the thresholds were determined manually via qualitative interpretation for the uranium mines observed in the study area. Quantitative data-driven sensitivity analysis could be used to optimize data thresholds as a future direction. Additional classes could be designed for other types of mines in the area to target the more elusive smaller, shallow, partially reclaimed uranium mines that were mined from the outcrop in the late 1950s and are potentially covered in vegetation and difficult to differentiate from gravel quarries (e.g., the Boso-Hackney Mine).

4.2. Mine Volume Estimation

The simple comparison of volume estimation approaches provides insights into factors that influence uncertainties and limitations when estimating mine feature volumes where the base elevations are unknown. When only post-mining topography is available, volume estimation accuracy could vary from site to site if the complexity of the terrain is over-simplified by using the cut-and-fill approach (i.e., elevations are sampled at mine feature polygon vertices and interpolated to then 'cut' a base height from which pit and pile volumes are estimated). The geomorphic difference between historical pre-mining and post-mining topography accounts for the complexity of the pre-mining terrain, however it is limited because the true mine feature base elevations are unverified. Additionally, the pre-mining DEM surfaces were determined via visual interpretation and it was beyond the scope of this study to determine the specific time step of the mosaiced historical NED topography for individual mine sites. The NED DEM was the best and the only available historical topographic information; the 10 m spatial resolution could introduce uncertainty when compared to the more detailed lidar-derived 50 cm bare earth elevation data.

The volume analysis based on applying the Cut and Fill method to post-mining bare earth topography consistently underestimated volumes when compared to the subset of reclaimed mine volume estimates derived from the geomorphic difference approach (Table 3). Historical pre-mining topographic data were not available for comparison of unreclaimed mine features in the study area. Although the high spatial resolution lidar delivered successful results for identifying and characterizing abandoned and reclaimed mines, post-mining topography and mine feature geometry may not be adequate to estimate mine waste volume for reclaimed mines. This is due to buried mine waste as documented by the RRC reclamation strategy based on flattening and reducing slope steepness of mine features. Volumes were calculated only for mine features, and therefore full areas of disturbance may need to be investigated in order to improve estimations of the presence of subsurface mine waste materials. The ability to map areas of disturbance from high spatial resolution lidar bare earth texture becomes an important tool for exploration and estimation of buried mine waste. Where available, ground geophysical methods can be used to determine subsurface characteristics of the underlying topography to achieve greater accuracies of mine waste estimation (e.g., [33] and references therein).

Conclusion

We studied known abandoned and reclaimed mine sites in order to develop a spatiotemporal mapping classification system, which utilizes multiple quantitative and qualitative remote sensing methods. This was done to: 1) identify uranium mine waste-rock, waste-water, and the total area of land disturbance due to mining; 2) differentiate abandoned and reclaimed mine features; and 3) derive mine feature volumes. This work ultimately contributes a better understanding of the life-cycle of mining activities on the Texas Coastal Plain landscape. The classification system was designed to help identify and differentiate mining features from non-mining features such as abandoned mine pits and pit lakes, abandoned waste-rock piles, as well as reclaimed mine pits, lakes and waste-rock piles. Lidar data were found to be an effective tool for achieving those goals.

As such, multiple lines of evidence were gleaned from analysis of the lidar 3-D elevation point cloud and derivative products including bare earth, slope, topographic contours, and overland-flow hydrography. Because our lidar datasets capture single points in time, we supplemented them with temporal analyses of LCLU change over time. The latter analyses included time-lapse and time-series spectral indices such as TCB, TCW, and TCG, which respectively detect land-cover brightness, wetness, and greenness. Temporal analysis of these spectral indices allowed us to explore the temporal life-cycle of mining in our study area. The mapping classification system was blind tested over a portion of the study area in order to assess the success of the approach for revealing uranium mine features. The classification system was successful in identifying large mines in the study area. Future work could benefit from fusing these methods with spectral-based mineral mapping and geophysical methods that can help detect radioactive and uranium-bearing minerals, and better characterizing the pre-mining topographic surface.

Author Contributions: Conceptualization, V.S., T.G. and B.H.; methodology, V.S., T.G., B.H., and D.W.; validation, V.S. and D.W.; formal analysis, V.S., D.W., and S.C.; investigation, V.S., T.G., B.H., and D.W.; data curation, VS, DW, SC; writing—original draft preparation, V.S., B.H., and D.W.; writing—review and editing, V.S., B.H., D.W., and T.G.; visualization, S.C. and V.S.; funding acquisition, T.G., B.H., and V.S.

Funding: Funding for this study was provided by the U.S. Geological Survey. This research received no external funding.

Data Availability Statement: The data presented in the article are published as a U.S. Geological Survey data release available at https://doi.org/10.5066/p9l50m8t.

Acknowledgments: The authors would like to thank the Railroad Commission of Texas for their willingness to provide guidance and resources describing the Texas coastal uranium mine lands and reclamation procedures. Any use of trade, firm, or product names is for descriptive purposes only and does not imply endorsement by the U.S. Government.

Conflicts of Interest: The authors declare no conflict of interest.

References

1. Hall, S.M.; Mihalasky, M.J.; Tureck, K.R.; Hammarstrom, J.M.; Hannon, M.T. Genetic and Grade and Tonnage Models for Sandstone-Hosted Roll-Type Uranium Deposits, Texas Coastal Plain, USA. *Ore Geology Reviews* **2017**, *80*, 716–753, doi:10.1016/j.oregeorev.2016.06.013.
2. Railroad Commission of Texas. *Texas Abandoned Mine Land Reclamation Projects*; Report; Railroad Commission of Texas - Surface Mining and Reclamation Division. **2002**, 11-24.
3. Dahlkamp, F.J. *Uranium Deposits of the World*, Springer Berlin Heidelberg, 2010; ISBN 978-3-540-78555-2.
4. Maus, V.; Werner, T. Impacts for Half of the World's Mining Areas Are Undocumented As the Race to Extract Minerals and Metals for Clean-Energy Technologies Accelerates, Researchers Must Take More Steps to Map and Study Mines Globally. *Nature* **2024**, *625*, 26–29, doi.org/10.1038/d41586-023-04090-3.
5. Hubbard, B.E.; Gallegos, T.J.; Stengel, V.G. Mapping Abandoned Uranium Mine Features along the South Texas Coastal Plain Using Worldview-3 Advanced Multispectral Imagery. *Minerals* **2023,** *13*, 839, doi:10.3390/min13070839.
6. Maxwell, A.E.; Shobe, C.M. Land-Surface Parameters for Spatial Predictive Mapping and Modeling. *Earth-Science Reviews* **2022**, *226*, 103944, doi:10.1016/j.earscirev.2022.103944.
7. Jing, L.; Zipper, C.; Li, S.; Donovan, P.; Wynne, R.; Oliphant, A.; Xia, Q. Character Analysis of Mining Disturbance and Reclamation Trajectory in Surface Coal-Mine Area by Time-Series NDVI. *Transactions of the Chinese Society of Agricultural Engineering (Transactions of the CSAE)* **2015**, *31*, doi:10.11975/j.issn.1002-6819.2015.16.033.

8. Gitau, F.; Maghanga, J.K.; Ondiaka, M.N. Spatial Mapping of the Extents and Volumes of Solid Mine Waste at Samrudha Resources Mine, Kenya: A GIS and Remote Sensing Approach. *Model. Earth Syst. Environ.* **2022**, *8*, 1851–1862, doi:10.1007/s40808-021-01192-7.
9. Gorelick, N.; Hancher, M.; Dixon, M.; Ilyushchenko, S.; Thau, D.; Moore, R. Google Earth Engine: Planetary-Scale Geospatial Analysis for Everyone. *Remote Sensing of Environ.* **2017**, *202*, 18–27, doi:10.1016/j.rse.2017.06.031.
10. Duque, J.F.M.; Zapico, I.; Oyarzun, R.; López García, J.A.; Cubas, P. A Descriptive and Quantitative Approach Regarding Erosion and Development of Landforms on Abandoned Mine Tailings: New Insights and Environmental Implications from SE Spain. *Geomorphology* **2015**, *239*, 1–16, doi:10.1016/j.geomorph.2015.02.035.
11. Blue Marble Geographics Global Mapper User Guide Available online: https://www.bluemarblegeo.com/knowledgebase/global-mapper-22-1/GlobalMapper.htm (accessed on 22 April 2024).
12. Brandt, J.; Moffett, L.L.; Waggoner, R. *South Texas Uranium District Abandon Mineland Inventory*; Report; Railroad Commission of Texas - Surface Mining and Reclamation Division **1994**, 186pp.
13. Dickinson, K.A. *Uranium Potential of the Texas Coastal Plain.* U.S. Geological Survey **1976**, Open-File Report 76-879, 11pp.
14. Fisher, W.L.; Proctor, C.V.; Galloway, W.E.; Nagle, J.S. Depositional Systems in the Jackson Group of Texas–Their Relationship to Oil, Gas and Uranium. Trans. *Gulf Coast Assoc. Geol. Soc.* **1970**, *20*, 234–261.
15. Eargle, D.H.; Dick, K.A. South Texas Uranium Deposits. *AAPG Bulletin* **1975**, *59*, doi:10.1306/83D91D21-16C7-11D7-8645000102C1865D.
16. Galloway, W.E. Uranium Mineralization in a Coastal-Plain Fluvial Aquifer System; Catahoula Formation, Texas. *Economic Geology* **1978**, *73*, 1655–1676, doi:10.2113/gsecongeo.73.8.1655.
17. Yang, L.; Jin, S.; Danielson, P.; Homer, C.; Gass, L.; Bender, S.M.; Case, A.; Costello, C.; Dewitz, J.; Fry, J.; et al. A New Generation of the United States National Land Cover Database: Requirements, Research Priorities, Design, and Implementation Strategies. *ISPRS Journal of Photogrammetry and Remote Sensing* **2018**, *146*, 108–123, doi:10.1016/j.isprsjprs.2018.09.006.
18. USDA-NASS Texas Cropland Data Layer (CDL) Available online: https://nassgeodata.gmu.edu/CropScape/ (accessed on 24 January 2024).
19. Mihalasky, M.J.; Hall, S.M.; Hammarstrom, J.M.; Tureck, K.R.; Hannon, M.T.; Breit, G.; Zielinski, R.A.; Elliott, B. *Assessment of Undiscovered Sandstone-Hosted Uranium Resources in the Texas Coastal Plain*. U.S. Geological Survey **2015**, Fact Sheet 2015-3069, Denver, CO, 4pp.
20. Murphy, T.; Brannstrom, C.; Fry, M. Ownership and Spatial Distribution of Eagle Ford Mineral Wealth in Live Oak County, Texas. *The Professional Geographer* **2017**, *69*, 616–628, doi:10.1080/00330124.2017.1298451.
21. Senkayi, A.L. Kaolinite, Opal-CT, and Clinoptilolite in Altered Tuffs Interbedded with Lignite in the Jackson Group, Texas. *Clays and Clay Minerals* **1987**, *35*, 281–290, doi:10.1346/CCMN.1987.0350405.
22. Warwick, P.D.; Crowley, S.S.; Ruppert, L.F.; Pontolillo, J. Tertiary Coals in South Texas: Anomalous Cannel-Like Coals of Webb County (Claiborne Group, Eocene) and Lignites of Atascosa County (Jackson Group, Eocene) - Geologic Setting, Character, Source-Rock and Coal-Bed Methane Potential. Chapter 3 - The San Miguel Lignite Deposit, Jackson Group (Eocene), South Texas. U.S. Geological Survey **1999**, Open-File Report 99-301, 23–36, https://doi.org/10.3133/ofr99301.
23. Strachan, C.L.; Raabe, K.L. Tailings and Mine Waste '98: Proceedings of the Fifth International Conference on Tailings and Mine Waste '98, Fort Collins, Colorado, USA; Balkema: Rotterdam, **1998**; 26–28, ISBN 978-90-5410-922-8.
24. Hubbard, B.E., Gallegos, T.J., Stengel, V.G., Hoefen, T.M., Kokaly, R.F., Elliott, B. Hyperspectral (Vnir-Swir) Analysis of Roll Front Uranium Host Rocks from Karnes and Live Oak Counties, Texas Coastal Plains. *Journal of Geochemical Exploration* **2023**, *257*, 107370, doi:10.1016/j.gexplo.2023.107370.
25. StratMap Ellis, Navarro, Wilson, & Karnes Counties Lidar, 2013-03-01 Available online: https://data.tnris.org/collection?c=6b475ef7-51e7-4e15-b652-4e942eafa85f#6.19/30.614/-97.062 (accessed on 6 April 2023).
26. U.S. Geological Survey South Central Texas Lidar, 2018-01-22 Available online: https://data.tnris.org/collection?c=77f928dc-298b-4b2e-9efd-8e2e16ece2c0#6.76/29.228/-98.5 (accessed on 6 April 2023).
27. Stengel, V.G.; McDowell, J.; Gallegos, T.J.; Hubbard, B.E.; Cahan, S. Data Associated with Using Lidar and Earth Observation Temporal Analysis to Explore and Characterize Uranium Mining on the South Texas Landscape. *U.S. Geological Survey* **2023**, *Data Release,* doi:https://doi.org/10.5066/P9L50M8T.
28. Jenson, S.K.; Domingue, J.O. Extracting Topographic Structure from Digital Elevation Data for Geographic Information System Analysis. *Photogrammetric Engineering and Remote Sensing* **1988**, *54*, 1,593-1,600.
29. Kennedy, R.; Yang, Z.; Gorelick, N.; Braaten, J.; Cavalcante, L.; Cohen, W.; Healey, S. Implementation of the LandTrendr Algorithm on Google Earth Engine. *Remote Sensing* **2018**, *10*, 691, doi:10.3390/rs10050691.

30. Crist, E.P. A TM Tasseled Cap Equivalent Transformation for Reflectance Factor Data. *Remote Sensing of Environment* **1985**, *17*, 301–306, doi:10.1016/0034-4257(85)90102-6.
31. The National Map: National Elevation Dataset (NED) 1 Arc-Second, Available online: https://nationalmap.gov/viewer.html (accessed on 17 August 2022).
32. Duval, J.S.; Schulz, K.A. Aerial Gamma-Ray Survey in Duval, McMullen, Live Oak, and Webb Counties, Texas. *U.S. Geological Survey* **1979,** *Professional Paper,* 43, *1123-A-D*. https://pubs.er.usgs.gov/publication/pp1123AD.
33. Karacan, C.Ö.; Erten, O.; Martín-Fernández, J.A. Assessment of Resource Potential from Mine Tailings Using Geostatistical Modeling for Compositions: A Methodology and Application to Katherine Mine Site, Arizona, USA. *Journal of Geochemical Exploration* **2023**, *245*, 107142, doi:10.1016/j.gexplo.2022.107142.